Efficient Removal of Copper(II) From Aqueous Solutions Using Polypyrrole Based Magnetic Nano-Adsorbent

Srivastava A.[1], Srivastava N.[2]* and Singh R.[3]
1. Department of Chemistry, GLA University, Mathura, U.P., INDIA
2. Department of Chemistry, D.D.U. Gorakhpur University, Gorakhpur, U.P., INDIA
3. Department of Chemistry, B.N. College of Engineering and Technology, Lucknow, U.P., INDIA
*neetusrivastav25@gmail.com

Abstract

Water contamination constitutes a substantial global issue that affects the environment. The discharge of manufacturing waste substantially contributes to this issue. Adsorption materials have demonstrated huge potential in wastewater treatment for the efficient removal of Cu(II). A polypyrrole-coated cobalt ferrite (PPy@$CoFe_2O_4$) magnetic nanosorbent is prepared via in situ polymerization of pyrrole on $CoFe_2O_4$ nanoparticles. Scanning electron microscopy (SEM) analysis demonstrated spherical nanoparticles with sizes around 50 nm, further supported by XRD data. The adsorption system adhered to a pseudo-second-order kinetic model with the equilibrium time being determined at 210 minutes. The Langmuir model accurately simulated the adsorption isotherms.

Under optimal conditions (pH - 6.0, volume - 40 ml, adsorbent dose – 40.0 mg and at 303 K temperature), the maximum monolayer adsorption capacity of PPy/$CoFe_2O_4$ is 199.6 mg g^{-1}. Negative $\Delta G°$ and $\Delta H°$ indicate spontaneous Cu(II) adsorption onto PPy/$CoFe_2O_4$, decreasing with temperature. These findings demonstrate that the PPy/$CoFe_2O_4$ composite is a highly effective adsorbent with broad potential applications for treating wastewater containing heavy metal ions.

Keywords: Conducting polymer, Pyrrole, Nanocomposite, Copper(II), Langmuir model, Kinetic model.

Introduction

A scarcity of clean drinking water continues to be a widespread issue in numerous countries. About a quarter of the global population lacks safe drinking water, ensuring potable water supply and leading to the tragic loss of 3.4 million lives annually, predominantly among children due to illnesses linked to water quality[6]. In recent years, wastewater production has notably surged due to rapid population expansion, heightened water usage, escalating industrial operations and intensified agricultural activities which have led to significant water contamination[25]. This contamination poses a severe risk to both human health and aquatic ecosystems[8]. Heavy metal ions in water pose a significant danger to water purity and can induce detrimental effects on biological systems. Even minimal amounts of metals can be detrimental to living organisms[20]. The reason behind this is the high propensity for heavy metals to accumulate in ecosystems and food webs[1].

Copper is known to be one of the major pollutants released by fertilizer, paper, electroplating, roofing, plumbing, air conditioning and electric wiring industry etc.[4,10,15,21]

Wastewater treatment facilities have demonstrated the capability to eliminate up to 80% of emerging contaminants; however, such high levels of efficiency are achievable only when integrated with advanced treatment methods. Advanced treatment techniques encompass a range of methodologies such as electrocoagulation, ion exchange, membrane separation, advanced oxidation processes, filtration, coagulation, adsorption, photocatalysis, electrodialysis and chemical precipitation[14]. Amongst these approaches, adsorption is acknowledged as a successful and potential technique because of its operational simplicity, high efficiency, cost-effectiveness and minimum production of secondary pollutants[8].

Conducting polymers comprise of conjugated π bonds and hold promising applications in fields such as biomedicine, corrosion prevention and gas sensing[8]. Conducting polymers such as polypyrrole offers a robust, sustainable approach to wastewater treatment, effectively removing heavy metals and contaminants through the presence of the functional group in its surface and tunable properties[3]. Although pure conducting polymers have limits, their integration with other materials to create smart composites mitigates these challenges. Conducting polymers (CPs) in these composites offer distinctive electrical, mechanical and pH-responsive characteristics, making them suitable for wastewater treatment[16]. These NCPs are esteemed for their stability, conductivity, facile synthesis and efficient regeneration, rendering them ideal substances for the extraction of heavy metals from wastewater[8].

This study involved the synthesis of a novel polypyrrole-coated cobalt ferrite magnetic nano adsorbent (PPy/$CoFe_2O_4$) by a simple *in situ* chemical polymerization technique. The PPy/$CoFe_2O_4$ nanocomposites were comprehensively characterized using various techniques including FTIR, XRD and Fe-SEM for surface morphological studies and their Cu(II) adsorption effectiveness from aqueous solutions was rigorously evaluated. Comparisons were conducted regarding the adsorption capacities of PPy/$CoFe_2O_4$, pure polypyrrole and virgin cobalt ferrite nanoparticles. Based on adsorption studies and instrumental assessment, we suggest the most

possible mechanistic pathway for the adsorptive elimination of Cu(II) by PPy/$CoFe_2O_4$ nanocomposite.

Material and Methods

Materials and Instrumentation: This investigation utilized analytical grade $Co(NO_3)_2{\cdot}6H_2O$, (≥ 99% pure) and $Fe(NO_3)_3{\cdot}9H_2O$, (≥99% pure) sourced from SRL. Chemicals including pyrrole (99% pure) from Spectrochem India, monoethanolamine (C_2H_7NO) 99% pure nitric acid (HNO_3), sucrose ($C_{12}H_{22}O_{11}$), ammonium persulfate (98%), sodium dodecyl sulfate (SDS) from SRL and $Cu(NO_3)_2$ from Merck India were procured. We formulated the Cu(II) stock solution in highly purified water by subjecting deionized water to double distillation.

The morphologies of $CoFe_2O_4$ and PPy/$CoFe_2O_4$ were examined using a Nova Nano 450 field FE-SEM. The FTIR spectra of $CoFe_2O_4$ and PPy/$CoFe_2O_4$ were obtained using a Nicolet 380 spectrometer within the 4000-400 cm^{-1} region utilizing KBr pellets. The XRD patterns of $CoFe_2O_4$ and PPy/$CoFe_2O_4$ were examined utilizing a D/MAX-2500PCX diffractometer with CuKα radiation in the 2θ range of 20 to 80 degrees. The atomic absorption spectrometry (Thermo scientific S4 series) was employed to quantify the Cu(II) concentration subsequent to adsorption experiments. The Malvern dynamic light scattering (DLS) instrument was employed to assess the Zeta potential of the PPy/$CoFe_2O_4$ composite.

Synthesis of Cobalt Ferrite ($CoFe_2O_4$) Nanoparticles: Employing the solution combustion method, we produced spherical cobalt ferrite nanoparticles. Initially, stoichiometric amounts of $Co(NO_3)_2{\cdot}6H_2O$ and $Fe(NO_3)_3{\cdot}9H_2O$ were solubilized in water. Monoethanolamine stabilized the nanoparticles inhibiting agglomeration by steric or electrostatic stabilization, assuring uniform size and minimizing clumping. The role of sucrose was to function as a fuel, delivering the heat required for the exothermic combustion reaction. In contrast, nitric acid acted as an oxidizing agent to facilitate the oxidation of both sucrose and metal ions. The oxidation process generated heat, triggering combustion and facilitating the breakdown of metal precursors, ultimately creating nanoparticles. The amalgamation was ignited and subsequently annealed at 600°C for 4 hours[11].

Synthesis of Polypyrrole-Coated Cobalt Ferrite (PPy/$CoFe_2O_4$) Magnetic Nanocomposite: The generation of a PPy/$CoFe_2O_4$ core-shell structure was achieved through the polymerization of pyrrole on $CoFe_2O_4$ nanoparticles using a chemical oxidative process at temperatures between 0-5 °C, with ammonium peroxy-disulfate serving as the oxidizing agent. 0.1 g of synthesized $CoFe_2O_4$ was carefully distributed in a separate beaker containing 100 ml of SDS (0.01 M) as a surfactant and subjected to sonication for 30 minutes with a probe sonicator. Subsequently, the cooled double-distilled liquid pyrrole (0.1 M) was meticulously added to the solution beaker, ensuring vigorous stirring at 1800 rpm throughout the process. A solution containing ammonium peroxy-disulfate, noted for its oxidizing properties, was introduced incrementally. The careful stirring was performed for 8 hours. The examination of the two separate layers was carried out. The upper layer, noted for its lightweight properties, consists exclusively of PPy, which was removed via decantation. The lower density layer consists of particles coated with PPy and $CoFe_2O_4$, filtered, rinsed with a 50% ethanol-water solution and dried for 20 hours at 70°C in an electric oven[26].

Adsorption Experiment: The adsorption of Cu(II) was investigated via batch methods. 200 mgL^{-1} $Cu(NO_3)_2$ was initially made and diluted to various concentrations (10, 20, 30, 40, 50, 60 and 70 mgL^{-1}). 40 mL of Cu(II) solution was typically administered to 40 mg of PPy/$CoFe_2O_4$ at the specified temperature. At different intervals, the PPy/$CoFe_2O_4$ was retrieved from the aqueous medium utilizing a permanent magnet and the residual Cu(II) concentration after adsorption was measured by atomic adsorption. Cu(II) adsorption at equilibrium and at any specific time, q_e (mg/g) and q_t (mg/g), along with the percentage elimination of Cu(II), was computed employing equations 1 and 2[17]. All experiments were conducted in triplicate.

$$q_e = \frac{(C_o - C_e) \times V}{m} \quad (1)$$

$$\% \text{ Removal} = \frac{(C_o - C_e) \times 100}{C_o} \quad (2)$$

The variables include the initial concentration of Cu(II) (C_o), the equilibrium concentration of Cu(II) (C_e), the mass of the adsorbent (m) and the volume of the solution (V). The optimum conditions for removing Cu(II) were established by analyzing the impact of Cu(II) concentration, pH (2.0-11.0), adsorbent/adsorbate quantity (5.0-80.0 mg/40 ml), contact time (2-300 min) and temperature (298-318 K) by batch experiments.

Results and Discussion

XRD analysis: The analysis of the composition and crystal structure of $CoFe_2O_4$ nanoparticles and the PPy/$CoFe_2O_4$ composite was conducted using X-ray diffraction (XRD) as illustrated in figure 1a. The XRD pattern reveals five unique characteristic peaks at 30°, 35.4°, 43.05°, 53.05°, 56.95° and 62.6°, aligning with the (220), (311), (400), (422), (511) and (440) planes of $CoFe_2O_4$ respectively[18,23]. The crystallite sizes of the $CoFe_2O_4$ nanoparticles and the PPy/$CoFe_2O_4$ composite were determined using the Debye-Scherrer equation, resulting in sizes of 17.5 nm and 18.0 nm respectively.

The distinct XRD peaks of $CoFe_2O_4$ indicate its excellent crystallinity whereas the reduced peak intensity observed in the PPy/$CoFe_2O_4$ composite implies that PPy effectively encapsulates the surface of the $CoFe_2O_4$ nanoparticles. Furthermore, distinctive peaks of PPy were detected in the range of 25° to 27°, which correspond closely with findings documented in prior studies[19].

SEM Analysis: Scanning electron microscopy (SEM) investigation demonstrated that cobalt ferrite nanoparticles, ranging from 20 to 50 nm in size, are uniformly distributed, as illustrated in figure 1b. Notwithstanding significant aggregation from magnetic dipole-dipole interactions, individual particles maintain their unique forms, signifying limited fusion. The rough surface texture indicates the successful fabrication of cobalt ferrite with uniform size and shape distribution, accomplished through meticulous regulation of precursor quantities and reaction parameters.

In the SEM images of the cobalt ferrite-polypyrrole composite, a homogenous polypyrrole coating envelopes the cobalt ferrite nanoparticles, forming a core-shell structure. This covering enhances particle size to between 50 and 100 nm, mitigating aggregation by restricting direct magnetic interactions (Figure 1c). The consistent surface seen in the composite underscores the efficacy of *in situ* polypyrrole polymerization, yielding a durable, well-dispersed material devoid of aggregation.

FTIR analysis: The FTIR spectra of cobalt ferrite nanoparticles reveal distinct vibration modes that signify the presence of the spinel structure (Figure 2). The two dominant bands identified in almost all spinel ferrites manifest within the 400-600 cm^{-1} range. The observed metal-oxygen bending vibrations in the tetrahedral sites are represented by a peak at 541 cm^{-1} which corresponds to the Fe-O bond. In contrast, the peaks at 461 cm^{-1} are associated with vibrations in the octahedral sites related to the Co-O bond[22]. The presence of additional peaks at 3747 cm^{-1} is indicative of O–H stretching vibrations, implying the existence of hydroxyl groups within the substance[9]. The peak observed at 2361 cm^{-1} may very well correspond to organic residues present within the material[3]. The appearance of these absorption peaks confirms the formation of the spinel ferrite structure.

Upon the introduction of PPy, the peak at 461 cm^{-1} experiences a shift to 467 cm^{-1} whereas the peak at 541 cm^{-1} shifts to 562 cm^{-1}[19]. The observed shift can be chiefly ascribed to the interplay between $CoFe_2O_4$ and PPy. The unique absorption band observed at 3438 cm^{-1} in PPy/$CoFe_2O_4$ nanocomposites can be ascribed to the stretching vibrations of N-H and O-H. The spectral feature noted at 758 cm^{-1} corresponds to the C-H wagging mode of PPy[12]. The vibrations associated with the C-H deformation and N-H in-plane deformation within the pyrrole ring account for the bands observed at 915 cm^{-1} and 1038 cm^{-1} respectively[2,28].

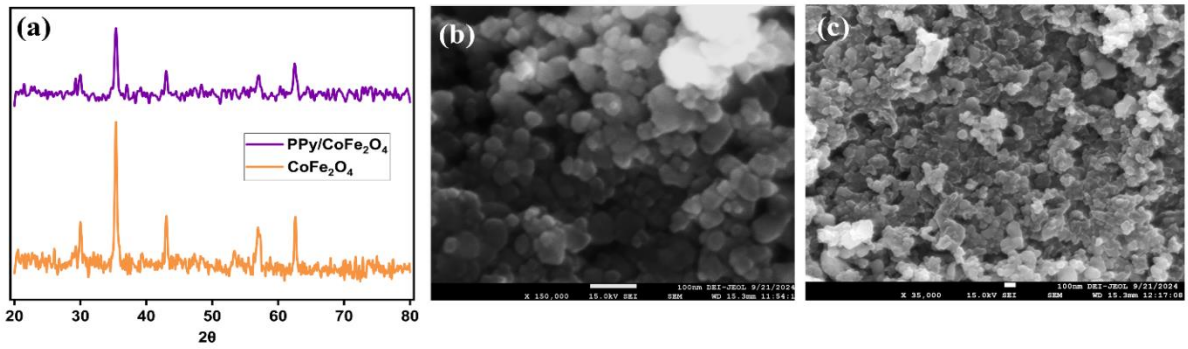

Figure 1: (a) XRD patterns of $CoFe_2O_4$ and PPy/$CoFe_2O_4$ (b) FE-SEM image of $CoFe_2O_4$ (c) FE-SEM image of PPy/$CoFe_2O_4$

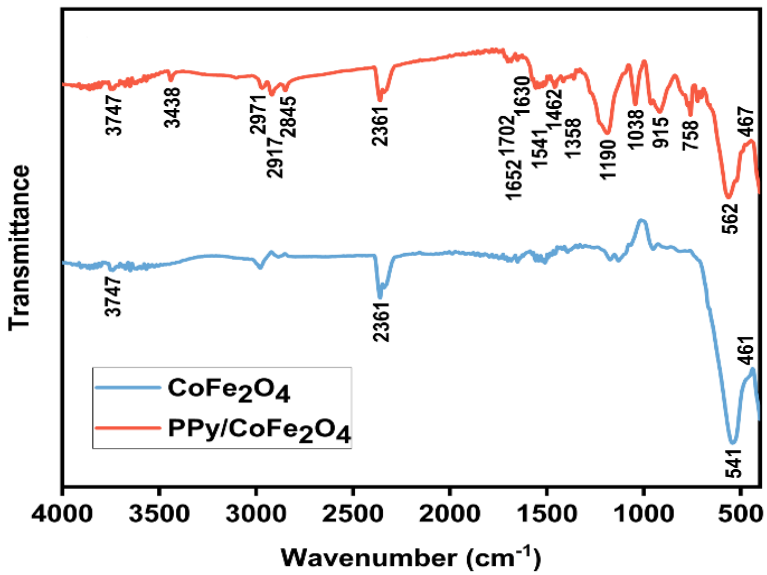

Figure 2: FTIR spectra of $CoFe_2O_4$ and PPy/$CoFe_2O_4$

The infrared spectrum elucidates the vibrations of C=N, C=C and C-C in PPy at 1652 cm^{-1}, 1541 cm^{-1} and 1462 cm^{-1} respectively. The FTIR peaks detected between 2845-2971 cm^{-1} in cobalt ferrite and PPy-cobalt ferrite signify C-H stretching vibrations of the alkyl groups inherent in the PPy structure or from residual organic precursors employed during the manufacturing process[23].

Influence of pH on Cu(II) removal: The main factor affecting adsorption effectiveness is pH, as it modifies the interface characteristics of both the adsorbate and adsorbent. This change affects the adsorbate's behavior in the reaction mixture as well as the deprotonation or protonation of different functional groups on the adsorbent surface. Multiple factors influence the effect of the solution's pH on Cu(II) adsorption on PPy/$CoFe_2O_4$. The electrostatic interaction between the adsorbate and adsorbent is an essential aspect to take into account.

The investigation of Cu(II) adsorption on PPy/$CoFe_2O_4$ was conducted across a pH range of 2.0-11.0, as depicted in figure 3a. It is noteworthy that for Cu(II), the adsorption capacity rises from 29.6 to 49.3 mg g^{-1} (59.3 % to 99.1 % removal) as the pH increases from 2.0 to 6.0, thereafter decrease in adsorption capacity was observed up to pH 11.0. As the pH of the solution rises, the columbic interactions between Cu(II) and PPy/$CoFe_2O_4$ increase, leading to improved adsorption capacities. Cu(II) experiences competition with H^+ ions for active sites on the adsorbent's surface at low pH, leading to the protonation of these sites. As a result, the adsorbent and Cu(II) experience lesser columbic interactions, which decrease adsorption.

Adsorption increases with increasing pH of solutions. At around neutral pH levels, the de-protonation of –C=N–H and Fe–OH groups takes place, leading to the formation of–C=N and Fe–O, which exhibit enhanced interactions with Cu(II)[8]. Consequently, the following experiments were conducted at pH 6.0. An identical pattern of change in adsorbent capacity with respect to the medium's pH has also been reported for the removal of the Cu(II)[13,24].

Influence of adsorbent dose on Cu(II) removal: Figure 3b demonstrates the effect of different adsorbent doses on the efficacy of removing Cu(II) from an aqueous solution. With an increase in the adsorbent dose (5.0 mg to 80.0 mg), there is a corresponding rise in removal efficiency, progressing from 49.6 % to 99.1 %. The enhancement is due to the increased surface area and the higher number of active sites available for adsorption. Beyond this point, however, the removal efficiency plateaus, as the concentration of Cu(II) ions becomes the limiting factor in the system. These findings underscore the strong affinity of PPy/$CoFe_2O_4$ composites for removing Cu(II).

Influence of Cu(II) concentration and contact time on Cu(II) removal: The adsorption behavior of Cu(II) on the PPy/$CoFe_2O_4$ composite was investigated throughout a temporal framework to determine the equilibrium point. Each experiment was rigorously reproduced in triplicate to ensure repeatability. Figure 4a illustrates the influence of contact duration and starting Cu(II) concentrations (20, 40 and 60 mg L^{-1}) on the adsorption capacity of PPy/$CoFe_2O_4$. The adsorption of Cu(II) initially increased rapidly, primarily due to the abundance of readily available active binding sites on the nanocomposite surface.

Nevertheless, with time, the adsorption rate progressively diminished. The reduced number of available active sites and the longer diffusion pathways that adsorbate molecules must follow later in the process, are the causes of the slowdown. Overall, the adsorption process began rapidly, transitioned into a slower removal phase and eventually reached equilibrium. In 210 minutes, the PPy/$CoFe_2O_4$ composite demonstrated the maximum adsorption capacity for Cu(II), suggesting that near complete equilibrium was attained.

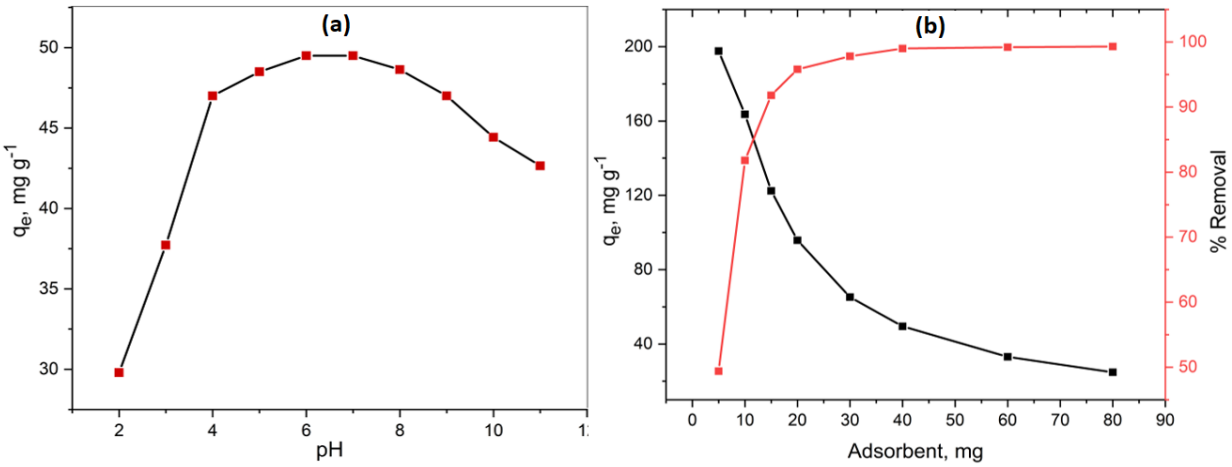

Figure 3: (a) Effect of pH on adsorption capacity of Cu(II) at [Cu(II)] = 50 mg/L, Adsorbent dose = 40 mg/40 ml, T = 303 K and Contact time = 300 min, (b) Effect of adsorbent dose on % removal and adsorption capacity of Cu(II) at [Cu(II)] = 50 mg/L, pH = 6.0, T = 303 K and Contact time = 300 min

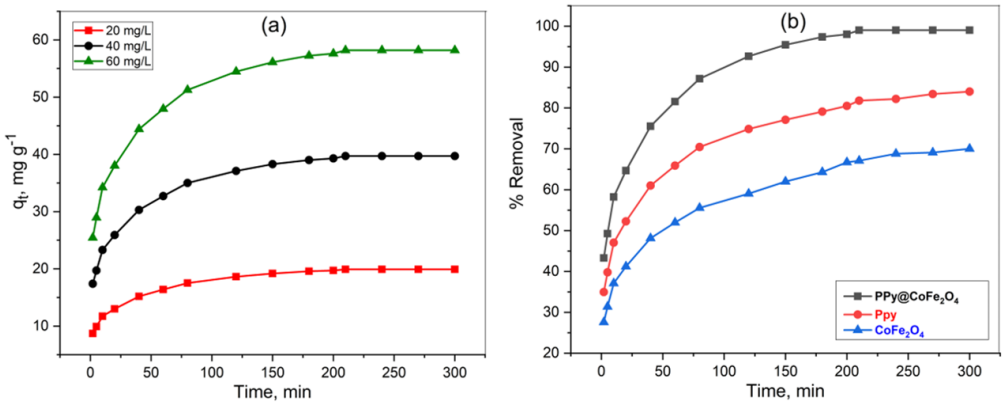

Figure 4: (a) Influence of [Cu(II)] and contact time on adsorption capacity of Cu(II) at adsorbent dose = 40 mg/40 ml, pH = 6.0, T = 303 K and Contact time = 300 min (b) Comparison of Cu(II) removal by $CoFe_2O_4$, PPy and PPy/$CoFe_2O_4$ at [Cu(II)] = 50 mg/L, adsorbent dose = 40 mg/40 ml, pH = 6.0, T = 303 K and Contact time = 300 min

The swift adsorption observed can be attributed to the readily accessible network structure of the PPy/$CoFe_2O_4$ composite, indicating that most adsorption sites are on the exterior surface, promoting rapid interaction with Cu(II). Cu(II) was efficiently adsorbed from aqueous solution by the PPy/$CoFe_2O_4$ composite, achieving equilibrium in 210 minutes at an initial concentration of 50 mg/L. Notably, approximately 80 % of Cu(II) was eliminated within the first 60 minutes, highlighting the efficiency and rapid action of the composite.

The adsorption equilibrium for Cu(II) onto the PPy/$CoFe_2O_4$ composite was attained within 210 minutes, demonstrating a remarkable removal efficiency of approximately 99.0 %, in contrast to the 77.8 % observed for cobalt ferrite nanoparticles under analogous conditions. In contrast, polypyrrole nanostructures exhibited a removal efficiency of merely 62.0 % after the same duration. The PPy/$CoFe_2O_4$ nano-composite exhibits superior removal effectiveness for Cu(II) compared to PPy and $CoFe_2O_4$ (Figure 4b).

Kinetics study: Time-dependent examinations were conducted to investigate the adsorption kinetics. The temporal data from the experiments were analyzed employing Lagergren's first-order model (Eq. 3) and Ho-McKay's second-order kinetic model (Eq. 4). These kinetics models' linearized equations are shown as follows: k_1 (min^{-1}) and k_2 (g^{-1} mg^{-1} min^{-1}) denote the rate constants for the pseudo 1st order and pseudo 2nd order respectively. Table 1 summarizes the parameters computed for these models.

$$\log(q_e - q_t) = \log q_e - \frac{k_1}{2.303} t \quad (3)$$

$$\frac{t}{q_t} = \frac{1}{k_2 q_e^2} + \frac{t}{q_e} \quad (4)$$

where q_t (mg/g) and q_e (mg/g) denote the quantity of Cu(II) adsorbed on PPy/$CoFe_2O_4$ at time t and at equilibrium respectively.

The removal of Cu(II) aligns closely with the pseudo-2nd order model (PSO), exhibiting R^2 values that approach 1. Comparing the results of the regression coefficients reveals that R^2 exhibits a value of 0.9998 in the analysis of second-order reaction kinetics (Figure 5b). On the other hand, in the context of pseudo-first-order (PFO) reaction kinetics, R^2 showed a value of 0.9798 (Figure 5a). Also, the adsorption capacity found with the second-order kinetics model (58.2 mg g^{-1}) closely approximates the experimental result (58.8 mg g^{-1}), especially when compared to the first-order model (31.03 mg g^{-1}). The results suggest that Cu(II) adsorption kinetics on PPy/$CoFe_2O_4$ follows second-order kinetic principles. Comparable pseudo-second-order kinetic behavior has also been noted in PS/Fe_3O_4@ PANI and SiO_2/$CuFe_2O_4$/polyaniline for Cu(II) removal[13,24].

Thermodynamic study: Thermodynamic parameters are critical in defining the characteristics and feasibility of the adsorption process. The adsorption capability and percentage removal of Cu(II) onto PPy/$CoFe_2O_4$ both significantly decline with increasing temperature. To analyze the thermodynamic parameters for Cu(II) adsorption on PPy/$CoFe_2O_4$ over a temperature range of 298 to 318 K, equations 5 to 7 were used. Equation 5 defines the relationship between the equilibrium constant (K_D) and the standard Gibbs free energy change (ΔG°) at a given temperature (T). Equation 6 describes the correlation of entropy (ΔS°) and enthalpy (ΔH°) of adsorption with ΔG° while equation 7 gives the expression for K_D.

$$\Delta G° = -RT \ln K_D \quad (5)$$

$$\ln K_D = -\left(\frac{\Delta G^o}{RT}\right) = -\left(\frac{\Delta H^o}{RT}\right) + \left(\frac{\Delta S^o}{R}\right) \quad (6)$$

$$K_D = \frac{C_{Ae}}{C_e} \quad (7)$$

where the equilibrium concentration of Cu(II) is C_e and the quantity of Cu(II) adsorbed on PPy/$CoFe_2O_4$ at equilibrium is C_{Ae}. The $\ln K_D$ vs. 1/T plot's slope and intercept yielded the values of ΔS° and ΔH°. The calculated values of the various parameters have been summarized in table 2.

The adsorption process for Cu(II) onto PPy/$CoFe_2O_4$ appears to be exothermic, as indicated by the negative ΔH° value.

Additionally, the negative ΔG° confirms that the adsorption of Cu(II) onto PPy/$CoFe_2O_4$ occurs spontaneously. However, as the temperature rises, the process becomes less favorable, evidenced by decreasing ΔG° values. The negative ΔS° value suggests a reduction in randomness at the solid-solution interface following adsorption. Similar trends in entropy and enthalpy during Cu(II) removal have also been observed in studies using PS/Fe_3O_4@ PANI and SiO_2/$CuFe_2O_4$/polyaniline as adsorbents[13,24].

Adsorption Isotherms: Selecting the appropriate isotherm model is crucial for understanding and optimizing adsorption processes. To analyze the equilibrium data for Cu(II) adsorption on PPy/$CoFe_2O_4$, various isotherm models were employed including the Freundlich and Langmuir models. The Freundlich model describes multilayer adsorption, indicating a range of affinities and adsorption energies across a heterogeneous surface. In contrast, the Langmuir model assumes monolayer adsorption at a fixed number of uniform, energetically similar sites, with minimal interactions among adsorbed molecules.

At equilibrium, the Langmuir adsorption equation for a monolayer of adsorbate adsorbed onto the adsorbent surface with finite active sites can be expressed as[5]:

$$\frac{C_e}{q_e} = \frac{1}{q_{max} K_L} + \frac{C_e}{q_{max}} \quad (8)$$

where the Langmuir constant is K_L (l/mg), the monolayer adsorbate adsorption performance or capacity is q_{max} (mg g^{-1}), the Cu(II) equilibrium concentration is C_e (mg L^{-1}) and q_e (mg g^{-1}) represents the amount of Cu(II) adsorbed on PPy/$CoFe_2O_4$ at equilibrium. The Langmuir constant describes the free energy involved in the adsorption process. Figure 6a depicts a graph of C_e against C_e/q_e, demonstrating a linear relationship.

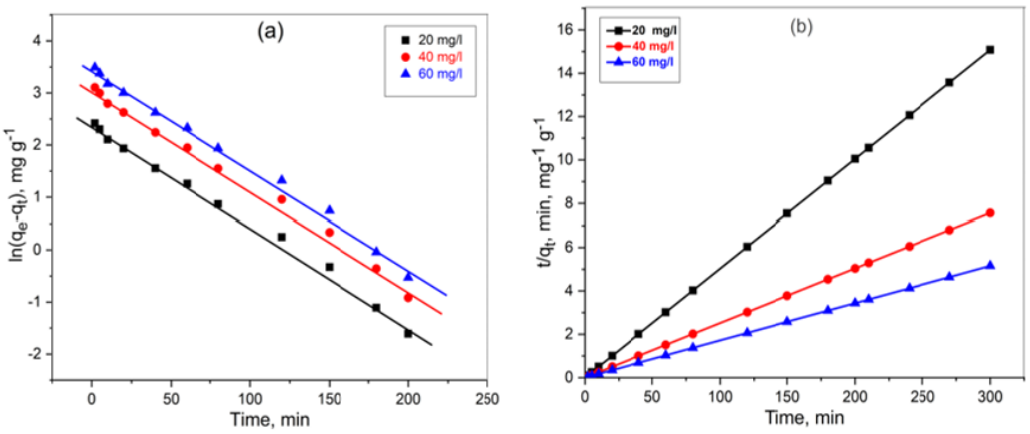

Figure 5: (a) First-order kinetics (b) Second-order kinetics for adsorption of Cu(II) by PPy/$CoFe_2O_4$ at [Cu(II)] = 50 mg/L, adsorbent dose = 40 mg/40 ml, pH = 6.0, T = 303 K and Contact time = 300 min

Table 1
Parameters calculated from PFO, PSO and IPD kinetic model

Kinetic Models	Parameters	Initial Cu(II) Concentration (mg/l)		
		20	40	60
Pseudo-first order kinetic	q_e (mg g^{-1})	10.71	20.90	31.03
	k_1 (min^{-1})	0.0196	0.0193	0.0195
	R^2	0.9843	0.9798	0.9853
Pseudo-second order kinetic	q_e (mg g^{-1})	19.6	39.1	58.2
	k_2 (g^{-1} mg^{-1} min^{-1})	0.251×10^2	1.72×10^2	0.521×10^2
	R^2	0.9994	0.9998	0.9996
q_e (mg g^{-1}) [Experimental]		20.1	39.9	58.8

Table 2
Thermodynamic parameters for Cu(II) adsorption onto PPy/$CoFe_2O_4$

Temp (K)	$\Delta H^{\#}$ kJ $mole^{-1}$	$\Delta S^{\#}$ J K^{-1} $mole^{-1}$	$\Delta G^{\#}$ kJ $mole^{-1}$
298	- 62.73	-168.83	- 10.426
303			- 11.575
308			- 12.615
313			- 13.593
318			-14.648

The K_L and q_{max} values can be ascertained by analyzing the intercept ($1/q_{max}\ K_L$) and slope ($1/q_{max}$) of the graph (Table 3). The plot in figure 6a illustrates the linearity, which strongly supports the validity of the Langmuir model. The experimental findings were consistent with the Langmuir model, indicating the uniform characteristics of the $PPy/CoFe_2O_4$ surface. This observation further demonstrated the adhesion of a single layer of Cu(II) molecule to the external $PPy/CoFe_2O_4$ surface. The previous report on Cu(II) adsorption onto PS/Fe_3O_4@ PANI and $SiO_2/CuFe_2O_4$/polyaniline yields comparable results[13,24].

The following equation is used to define a dimensionless equilibrium parameter R_L which is used to assess the adsorption's favorability:

$$R_L = \frac{1}{1 + K_L C_o} \quad (9)$$

The initial concentration of Cu(II) is indicated as C_o (mg L^{-1}), while the Langmuir constant is represented as K_L. Based on the R_L value, the isotherm type can be classified as irreversible ($R_L > 1$), unfavorable ($R_L = 0$), favorable ($0 < R_L < 1$), or linear ($R_L = 1$)[27].

The Freundlich model, more suited for heterogeneous surfaces, describes multi-layer adsorption rather than a plateau-type saturation[7]. Its mathematical form is:

$$\log q_e = \log K_F + \frac{1}{n} \log C_e \quad (10)$$

In this context, q_e (mg g^{-1}) denotes the quantity of adsorbed Cu(II) on $PPy/CoFe_2O_4$ at equilibrium while C_e (mg L^{-1}) indicates the equilibrium concentration of Cu(II). Furthermore, n and K_F represent the respective constants of the Freundlich isotherm model. Figure 6b illustrates the linear correlation between $\ln C_e$ and $\ln q_e$. Table 3 shows the values of K_F and n, which were computed from the intercept ($\ln K_F$) and slope ($1/n$) of the plot. The value of n indicates the adsorption's favorability. There is a typical Langmuir isotherm if the value of $1/n$ is smaller than 1[5].

The adsorption of Cu(II) on $PPy/CoFe_2O_4$ was found to align strongly with the Langmuir isotherm model, as evidenced by a high R^2 value of 0.9981. This high correlation suggests an even distribution of active adsorption sites across the $PPy/CoFe_2O_4$ surface.

Additionally, the Langmuir isotherm's dimensionless constant R_L ranged between 0 and 1, while the Freundlich constant $1/n$ was less than 1, supporting the thermodynamic favorability of the process.

Conclusion

The current study demonstrates that the $PPy/CoFe_2O_4$ nanocomposite serves as an effective adsorbent for the removal of Cu(II) from aqueous solutions. The variables involved, the solution's pH, the interaction time between adsorbent and adsorbate, the dose of $PPy/CoFe_2O_4$ and the initial Cu(II) concentration, have substantially impacted the adsorption process.

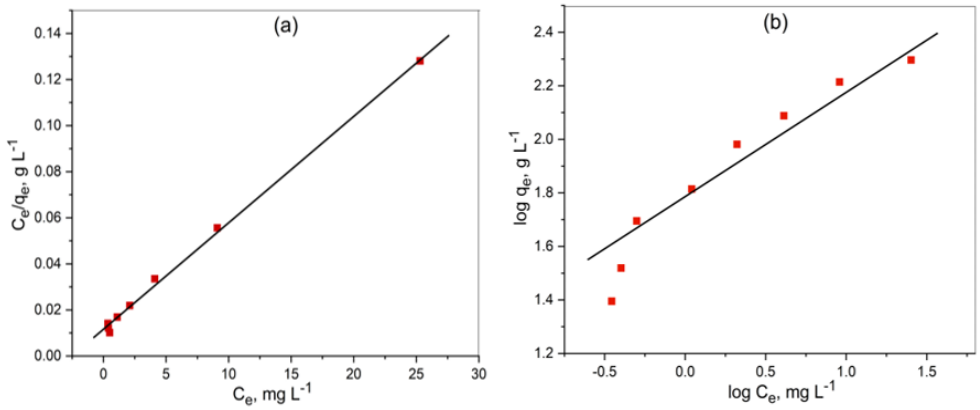

Figure 6: Plot of (a) Langmuir isotherm model (b) Freundlich isotherm model for the adsorption of Cu(II) on $PPy/CoFe_2O_4$

Table 3
Langmuir, Freundlich and Temkin isotherm constants

Isotherm	Constant Values
Langmuir	q_{max}(mg/g) = 204.1
	K_L(L/mg) = 0.426
	R^2 = 0.9981
	R_L = 0.193 - 0.034
Freundlich	K_F (mg/g) = 55.97
	1/n = 0.4621
	R^2 = 0.9321

The optimal pH value for the adsorption of Cu(II) was determined to be 6.0. The PPy/$CoFe_2O_4$ composite exhibited excellent adsorption capabilities for Cu(II) removal. The isotherm investigation revealed that the Langmuir model most accurately represented the equilibrium data for Cu(II), exhibiting a maximum monolayer sorption capacity of 199.6 mg g^{-1} at 303 K. A pseudo-second-order kinetic model was demonstrated to be applicable for Cu(II) adsorption, with the equilibrium period established within 210 minutes. In conclusion, PPy/$CoFe_2O_4$ is an extremely effective magnetic nanosorbent, characterized by outstanding reusability and facile magnetic separability, demonstrating significant potential for the removal of heavy metal ions from wastewater.

References

1. Ali A. and Naima M., Emerging insights into the impacts of heavy metals exposure on health, reproductive and productive performance of livestock, *Frontiers in Pharmacology,* **15**, 1375137 **(2024)**

2. Ali H. and Ismail A.M., Fabrication of Magnetic Fe_3O_4/ Polypyrrole/Carbon Black Nanocomposite for Effective Uptake of Congo Red and Methylene Blue Dye: Adsorption Investigation and Mechanism, *Journal of Polymers and the Environment*, **31**, 976-998 **(2023)**

3. Aziz C. and Azhdar B., Synthesis of dysprosium doped cobalt ferrites nanoparticles by solgel auto-combustion method and influence of grinding techniques on structural, Morphological and magnetic properties, *Journal of Magnetism and Magnetic Materials*, **542**, 168577 **(2022)**

4. Bhuiyan M.A.H., Parvez L., Islam M.A., Dampare S.B. and Suzuki S., Heavy metal pollution of coal mine-affected agricultural soils in the northern part of Bangladesh, *Joirnal of Hazardous Materrials*, **173**, 384-392 **(2010)**

5. Budhiraja T., Rawat V., Kimothi S., Dumka U.C. and Gupta R., Low temperature physical activation of raw charcoal for excellent dye adsorption kinetics, *Fullerenes Nanotubes and Carbon Nanostructure*, **33**, 1-15 **(2024)**

6. Campbell R., Xiao B. and Mangwandi C., Production of activated carbon from spent coffee grounds (SCG) for removal of hexavalent chromium from synthetic wastewater solutions, *Journal of Environmental Management*, **366**, 121682 **(2024)**

7. Freundlich H., Over the Adsorption in Solution, *International Journal of Research in Physical Chemistry and Chemical Physics*, **57**, 387-470 **(1906)**

8. Goswami M.K. et al, Recent advances in conducting polymer-based magnetic nanosorbents for dyes and heavy metal removal: fabrication., applications. and perspective, *Environmental Science and Pollution Research*, **30**, 73031-73060 **(2023)**

9. Hair M.L., Transmission Infrared Spectroscopy for High Surface Area Oxides., in Vibrational Spectroscopies for Adsorbed Species, *American Chemical Society*, **137**, 1-11 **(1980)**

10. Hama Aziz K.H., Mustafa F.S., Omer K.M., Hama S., Hamarawf R.F. and Rahman K.O., Heavy metal pollution in the aquatic environment: efficient and low-cost removal approaches to eliminate their toxicity: a review, *RSC Adv*, **13**, 17595-17610 **(2023)**

11. Houshiar M., Zebhi F., Razi Z.J., Alidoust A. and Askari Z., Synthesis of cobalt ferrite (CoFe2O4) nanoparticles using combustion., coprecipitation. and precipitation methods: A comparison study of size., structural and magnetic properties, *Journal of Magnetism and Magnetic Materials*, **371**, 43-48 **(2014)**

12. Hussain D., Siddiqui M.F., Shirazi Z. and Khan T.A., Evaluation of adsorptive and photocatalytic degradation properties of FeWO/polypyrrole nanocomposite for rose bengal and alizarin red S from liquid phase: Modeling of adsorption isotherms and kinetics data, *Environmental Progress and Sustainable Energy*, **41**, e13822 **(2022)**

13. Li Y., Qiu J., Ye S., Wang L., Yang C., Sun P. and Wang C., Facile fabrication of PS/Fe_3O_4@ PANi nanocomposite particles and their application for the effective removal of Cu^{2+}, *New Journal of Chemistry*, **41**, 14137–14144 **(2017)**

14. Liu Y., Wang H., Cui Y. and Chen N., Removal of Copper Ions from Wastewater: A Review, *International Journal of Environmental Research and Public Health*, **20**, 3885 **(2023)**

15. Moore R.Z., Wilson V., Hou A. and Meng G., Source of lead pollution, its influence on public health and the countermeasures, *International Journal of Health, Animal Science and Food Safety*, **2**, 18-31 **(2015)**

16. Namsheer K. and Rout C.S., Conducting polymers: a comprehensive review on recent advances in synthesis, properties and applications, *RSC Advances*, **11**, 5659-5697 **(2021)**

17. Patra C., Shahnaz T., Subbiah S. and Narayanasamy S., Comparative assessment of raw and acid-activated preparations of novel Pongamia pinnata shells for adsorption of hexavalent chromium from simulated wastewater, *Environmental Science and Pollution Research*, **27**, 14836-14851 **(2020)**

18. Pourgolmohammad B., Masoudpanah S.M. and Aboutalebi M.R., Synthesis of CoFe2O4 powders with high surface area by solution combustion method: Effect of fuel content and cobalt precursor, *Ceramics International*, **43**, 3797-3803 **(2017)**

19. Ren J., Wang C., Zhang H., Liu X. and Yan T., Magnetic Core@Shell Fe3O4@Polypyrrole@Sodium Dodecyl Sulfate Composite for Enhanced Selective Removal of Dyestuffs and Heavy Metal Ions from Complex Wastewater, *Langmuir*, **39**, 10098-10111 **(2023)**

20. Sable H., Singh V., Kumar V., Roy A. and Pandit S., Toxicological and bioremediation profiling of nonessential heavy metals (mercury., chromium., cadmium., aluminium) and their impact on human health: A review, *Toxicologie Analytique et Clinique*, **36**, 205-234 **(2024)**

21. Sailer J., Nagel J., Akdogan B., Jauch A.T., Engler J., Knolle P.A. and Zischka H., Deadly excess copper, *Redox Biology*, **75**, 103256 **(2024)**

22. Shyamaldas, Bououdina M. and Manoharan C., Dependence of structure/morphology on electrical/magnetic properties of hydrothermally synthesised cobalt ferrite nanoparticles, *Journal of Magnetism and Magnetic Materials*, **493**, 165703 **(2020)**

23. Soltani-Nezhad S., Mashreghi A., Hasani S., Rezvan M.T. and Ziarati A., Application of Taguchi method to optimize the properties of cobalt ferrite nanoparticles doped by Ca^{2+} and Gd^{3+}, *Inorganic Chemistry Communications*, **159**, 111759 **(2024)**

24. Taleb M.A., Kumar R., Al-Rashdi A.A., Seliem M.K. and Barakat M., Fabrication of SiO_2/$CuFe_2O_4$/polyaniline composite: a highly efficient adsorbent for heavy metals removal from aquatic environment, *Arabian Journal of Chemistry*, **13**, 7533–7543 **(2020)**

25. Tundwal A., Kumar H., Binoj B.J., Sharma R. and Kumari R., Conducting polymers and carbon nanotubes in the field of environmental remediation: Sustainable developments, *Coordination Chemistry Review*, **500**, 215533 **(2024)**

26. Wang W., Ren J., Wang C., Zheng M. and Ma Y., Magnetic FeO/polypyrrole-salicylaldehyde composite for efficient removal of Mn (VII) from aqueous solution by double-layer adsorption, *Journal of Applied Polymer Science*, **139**, e52515 **(2022)**

27. Weber T.W. and Chakkravorti R.K., Pore and solid diffusion models for fixed bed adsorbers, *American Institute of Chemical Engineers*, **20**, 228 **(1974)**

28. Yuan L., Wan C., Ye X. and Wu F., Facial Synthesis of Silver-incorporated Conductive Polypyrrole Submicron Spheres for Supercapacitors, *Electrochimca Acta*, **213**, 115-123 **(2016)**.

(Received 13th December 2024, accepted 15th February 2025)